(This article is a preprint of the final article that appeared in the 1993 IEEE Ultrasonics Symposium Proceedings, pp. 1107-1112)

ELECTROMECHANICAL MODELING USING EXPLICIT TIME-DOMAIN FINITE ELEMENTS

G.L. Wojcik, D.K. Vaughan, N. Abboud*, J. Mould, Jr.

Weidlinger Associates
4410 El Camino Real, Suite 110, Los Altos, CA, U.S.A. 94022
*333 Seventh St., New York, NY, U.S.A. 10001

ABSTRACT

Piezoelectric transducers serve as electromechanical transceivers in sonar, medical imaging, NDE, and signal processing systems. Despite their relative technical maturity, many opportunities for improvement and innovation remain. To best exploit these opportunities we need to augment standard design procedures based on 1D models and prototype experiments. Rigorous finite element computer modeling offers a powerful adjunct to conventional methods, yet it has enjoyed only limited acceptance despite major industry efforts. One reason is reliance on traditional *implicit* numerical algorithms for frequency-domain analysis or time integration. We present an alternative mixed *explicit/implicit* algorithm for direct time-domain integration of the 2D or 3D electromechanical equations. On the same workstation it affords about two orders of magnitude faster solutions or larger models than do available implicit codes, and makes desktop transient device modeling practical. This paper reviews algorithms, presents validation calculations, describes 2D and 3D array simulations, explores associated wave propagation issues, and considers future directions.

INTRODUCTION

Piezoelectric transducers convert electrical signals to mechanical signals and vice versa. They serve as transmitters and receivers in imaging systems for sonar, medical, and NDE (nondestructive evaluation) applications, as well as in nonimaging applications like SAW (surface acoustic wave) devices in signal processing, e.g., see [1]. The piezoelectric transducer market is broad and the technology, despite its relative maturity, has great potential for improvement and innovation.

One of the most technically demanding applications is ultrasound (ultrasonic) medical imaging. Operational emphasis for imaging transducers is broadband (impulsive) rather than narrowband (continuous wave). Transducers are currently available for diagnostic imaging and Doppler velocity measurement, e.g., [2], as well as a host of specialty appli-cations (intracavity, biopsy, etc.) including disease treatment (lithotripsy, hyperthermia, tissue ablation). Over the last two decades the ultrasound industry has done a remarkable job developing and refining these devices using a combination of semi-analytical design procedures and prototype experiments. However, it is apparent to many that conventional design methods are approaching practical limits of effectiveness. The industry has been slowly recognizing discrete numerical modeling on the computer as a complementary solution [3-9].

Today nearly all of the major ultrasound system companies are experimenting with finite element models using commercial packages like ANSYS® [10] or by writing their own codes, e.g., Lerch [11,12]. Most have enjoyed only limited success at significant development and/or simulation costs. We suggest that the main source of difficulty is universal reliance on classical *implicit* algorithms for frequency-domain and time-domain analysis—based on related experience with shock and wave propagation analyses, e.g., [13,14]. In general, *implicit* algorithms are best suited to linear static problems, steady state vibrations, and low frequency dynamics. A much better choice for transient phenomena, linear or nonlinear, is an *explicit* time-domain algorithm, which exploits the hyperbolic (wave) nature of the governing differential equations, e.g., see [15].

This paper focuses on our recent experience implementing and applying an *explicit* time-domain algorithm for piezoelectric transducers under an NSF SBIR grant [16]. We review the algorithmic issues, present validation calculations, describe 2D and 3D transducer array simulations, briefly explore some wave propagation issues, summarize, and conclude with a brief mention of modeling alternatives and future directions. The algorithmic approach described here permits practical solution of transducer problems with thousands to millions of elements in minutes to a few hours on a workstation with 64 MBytes or more of random access memory. Demonstrated computational advantages over conventional *implicit* algorithms are typically factors of 100 or more in speed and 100-1000 in model size, on the same workstation.

ALGORITHM BACKGROUND

The finite element method reduces the electromechanical partial differential equations (PDEs) over the model domain to a system of ordinary differential equations (ODEs) in time. This is done using one of the nearly equivalent integral formalisms—virtual work, weak form, Galerkin's method, weighted residuals—or less formally, using point-wise enforcement of the conservation and balance laws. The result is that spatial derivatives in the PDEs are reduced to a summation of "elemental" systems of linear algebraic equations on the unknown field values at nodes of the finite element discretization. The continuum elements used here are 4 node quadrilaterals in 2D and 8-node hexahedrons in 3D. The unknown field over an element is represented by low order shape functions determined by nodal (corner) values, i.e., bilinear in 2D and trilinear in 3D. Using a minimum of 15 elements per wavelength limits wave dispersion errors to less than 1%. Experience has shown these choices to offer the most robust basis for large-scale wave propagation analysis [14] in structural and isotropic or anisotropic continuum models.

The electromechanical finite element equations are derived from the piezoelectricity constitutive relations and the equations of mechanical and electrical equilibrium [17]. Applying the formalism and "adding" or assembling the local equations for all elements in the model yield the global system of ODEs

$$M_{uu}\frac{d^2u}{dt^2}+C_{uu}\frac{du}{dt}+C_{u\psi}\frac{d\psi}{dt}+K_{uu}u+K_{u\phi}\phi=F \quad (1)$$

$$K_{u\phi}^{T}u-K_{\phi\phi}\phi=Q \quad (2)$$

$$M_{\psi\psi}\frac{d^2\psi}{dt^2}-C_{u\psi}^{T}\frac{du}{dt}+C_{\psi\psi}\frac{d\psi}{dt}+K_{\psi\psi}\psi=0 \quad (3)$$

governing elastic (1), electric (2), and acoustic (3) fields. Note that the mechanical equations, (1) and (3), are dynamic while the electric equation, (2), is quasi-static [17]. Global unknowns u, ϕ, and ψ are, respectively, the elastic displacement vector, the electric potential vector, and the velocity potential vector, while F is the applied force vector and Q is the charge vector. These vectors are defined by field values at all nodes in the model. Coefficients M, C, and K denote the various uncoupled and coupled "mass," "damping," and "stiffness" matrices, respectively. To solve these ODEs it is necessary to make assumptions about the temporal behavior of the electromechanical phenomena. Frequency-domain solutions assume time-harmonic behavior, effectively removing time as an independent variable. Time-domain solutions assume general temporal evolution of the system, requiring step-by-step integration of the equations. Integration can be done using either an *implicit* or an *explicit* method [18].

For frequency-domain analysis of (1)-(3) the unknowns become $u=\hat{u}e^{i\omega t}$, $\phi=\hat{\phi}e^{i\omega t}$, and $\psi=\hat{\psi}e^{i\omega t}$, which yields three inhomogeneous systems of implicit equations for $\hat{u}$, $\hat{\phi}$, and $\hat{\psi}$. Direct solution by Gaussian elimination is only practical in 2D because 3D typically leads to prohibitively large system bandwidth and memory needs. The alternative is an iterative solution. If the system is symmetric and positive definite (positive eigenvalues) then the conjugate gradient (CG) method is appropriate. In practice, material attenuation and radiation boundary conditions make the system of equations complex, non-hermitian, and typically indefinite, requiring a more general iterative solver, like GMRES [19] or the new, more robust QMR algorithm [20].

When transient signals are of principal interest, the most direct solution method is step-by-step integration in time. There are many ways to evaluate the current solution from known results at previous time steps. *Implicit* methods couple the current solution vector, hence, the global system of equations must be solved at each timestep. Their advantage is unconditional stability with respect to time step. By contrast, *explicit* methods decouple the current solution vector and eliminate the global system solve, but they are only conditionally stable, i.e., there is a time step limit (CFL condition, [21]) above which the method is unstable. The caveat for *implicit* integration of wave phenomena is that solution accuracy requires a time step smaller than one-tenth the period of the highest frequency to be resolved. This is close to the CFL stability limit for *explicit* methods and effectively removes the principal advantage of *implicit* integration.

Explicit integration of (1) and (3) involves diagonalizing the uncoupled mass and damping matrices, M_{uu}, $M_{\psi\psi}$, C_{uu}, $C_{\psi\psi}$, using nodal lumping, replacing the time derivatives with finite differences, and integrating using a central difference scheme (2nd order accurate). For stability the time step must be smaller than the shortest wave transit time across any element (CFL condition). This follows from the hyperbolic (wave) nature of the original PDEs, i.e., during time step Δt the field at a point is only influenced by the field at neighboring points within a sphere of radius $\Delta x=c_p\Delta t$ where c_p is the fastest local wave speed. Therefore, for $\Delta t<\Delta x/c_p$ nodal fields are decoupled during a single time step and can be integrated independently.

The point is that it is possible to eliminate the manipulation and solution of large systems of electromechanical equations by integrating (1) and (3) *explicitly* in time for u and ψ using ϕ from the previous time step, and then solving (2) *implicitly* for the new ϕ from u using a preconditioned CG iteration (diagonal scaling). Thus, the algorithm operates on an element-by-element basis, where elemental contributions are accumulated in intermediate global vectors, e.g., the nodal force or charge vectors, and the algorithm processes these vectors only. This is equivalent to matrix-vector arithmetic without actually forming the matrix, which facilitates vectorization and parallelization.

An important issue in transducer modeling is frequency-dependent material damping. Regardless of the solution technique, fundamental assumptions must be made about the structure of the uncoupled damping matrices in (1) and (3). The two most convenient damping models are mass-proportional (viscous, $\propto 1/\omega$) and stiffness-proportional ($\propto \omega$), e.g., Lerch [12]. A linear combination is called Rayleigh damping. In the frequency-domain, coefficients are simply chosen to give the required damping at each frequency calculated. In the time-domain, constant coefficients yield damping that is inversely or directly proportional to frequency, or a linear combination. We also use a material-dependent, three-parameter viscoelastic damping model, e.g., see [22]. Proper choice of viscosity constants and a relaxation time yields a damping maximum at the selected frequency and smooth fall-off. Therefore, viscoelastic models may be superposed to yield a discrete spectrum of relaxation times that represent specified damping behavior over a limited frequency range, but at significant cost in memory.

The final issue is radiation boundary conditions. It is always necessary to truncate the finite element model in space because of limited computer memory. This is a fundamental problem in numerical simulation [23] and requires special boundary conditions to reduce spurious reflections (grid truncation error). Time-domain continuum conditions are typically derived from the one-way wave equation, with an ad hoc approximation used to fit the discretization. Higher order implementations tend to degrade in 3D vector domains due to this ad hoc discreti-zation. A new and better approach operates directly on the finite element equations using the general relation between spatial and temporal derivatives at an arbitrary wavefront. This yields boundary node velocity in terms of its derivatives over the element and stresses within the boundary element [24]. The condition performs as well as a 4th order paraxial absorber [25], with lower computational overhead and less impact on stability.

VALIDATION CALCULATIONS

The *explicit*/*implicit* algorithm was verified against experiments to check accuracy and robustness of the mixed integration scheme. We simulated impedance sweeps on a suite of rectangular piezoelectric bars in air, with width/thickness, i.e., aspect ratio, AR=0.195, 0.381, 0.455, 0.597, 0.740, 0.890. 1.99 & 4.97. Lengths were nominally 21 thicknesses. Data consisted of amplitude and phase plots (H-P 4194 Network-Im-

pedance Analyzer) of complex impedance (voltage/current) from 2.0 to 7.0 or 8.0 MHz. Recall, minima and maxima occur at the short circuit resonances and open circuit antiresonances, respectively. Two types of impedance calculations were considered, driven by either time-harmonic or transient voltage.

Bars were cut from a uniform, thin sheet of poled piezoelectric ceramic similar to PZT-5H and suspended in air by wires to plated electrodes on the top and bottom (poling) faces. Mechanical loading by the air and the thin electrodes was negligible. Complete electromechanical properties were not measured but simply scaled from PZT-5H, based on the measured V_L. An estimate of mechanical damping was made by matching the antiresonance of the AR=0.195 model to the data near its minimum. This gave a damping ratio of 1.89% of critical ($\varepsilon = 0.0189$).

2D and 3D prism models were discretized into 25 finite elements through the thickness and a minimum of 15 through the width, keeping element aspect ratio close to unity. Boundary conditions on all sides were stress-free since the mechanical impedance of air was insignificant at the frequencies considered. Models were driven by time-harmonic ($\sin\omega t$) or transient voltage (250 nsec square wave) applied abruptly at t = 0 on nodes corresponding to the electrode locations. Current was calculated by summing the time rate of change of charge at these nodes. Comparisons of 2D and 3D simulations for both the AR=0.195 and AR=1.99 samples showed virtually no difference in calculated impedance, hence, 2D models were used. This is not to say that prism response is strictly 2D, only that (long) bar impedance is insensitive to 3D end effects.

Sinusoidal voltage simulations were run to steady state, amplitude and phase of current were determined from time histories, impedance was calculated, and the process was repeated at about 200 frequencies to capture details around all resonances and antiresonances. This is equivalent to using an *implicit* frequency-domain code. However, a time-domain code can also yield impedance from a transient calculation by dividing Fourier transforms of voltage and current. The only requirement is that the applied voltage transient must contain significant energy over the frequencies of interest. Differences between discrete frequency and transient approaches are due, primarily, to the damping models assumed for each.

Figure 1 shows cross-plots of the measured and calculated impedance amplitude (upper) and phase (lower) for the AR=0.89 case. There is generally good agreement except that the calculated higher mode frequencies are shifted upward by 0.1-0.2 MHz. Both discrete frequency and transient/FFT impedance calculations are shown. Damping is constant ($\varepsilon = 0.0189$) at each frequency for the discrete case, while mass-proportional damping matches this value at 2.5 MHz and varies as inverse frequency for the transient/FFT calculation. The latter approach is preferred for these experiments because it is faster by a factor of 300 or so and lower damping at higher frequencies appears to fit the data better. Similar agreement was found between simulated and experimental data for all aspect ratios less than unity, (see Fig. 2 for AR=0.195, 0.381.)

Significant discrepancies were found for the higher aspect ratio bars, Figure 3, although qualitative agreement was still good. Higher aspect ratio bar vibrational modes are more complicated and dependent on the full constitutive matrices, i.e., more sensitive to errors in electromechanical properties. Prompted by the crude estimates used here, simple parameter

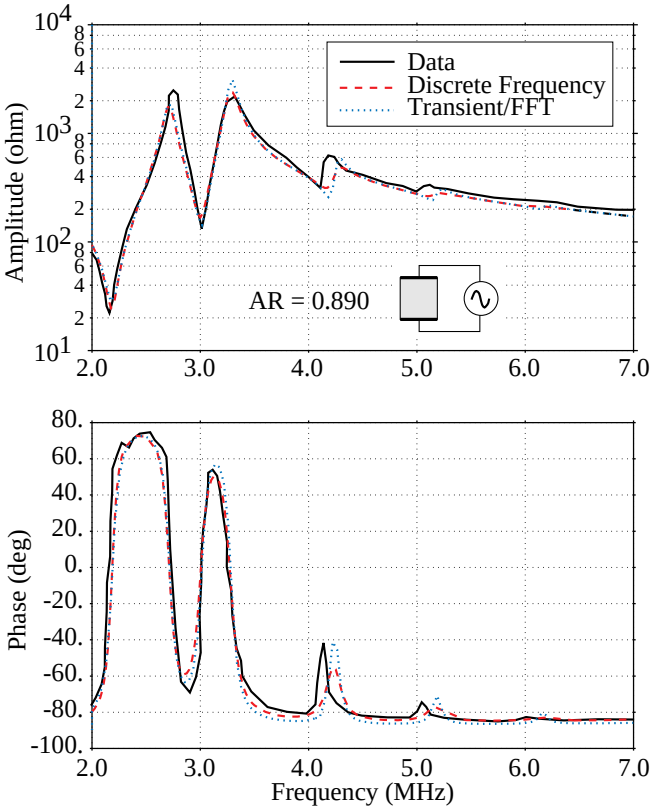

Figure 1. Electrical impedance amplitude and phase for the AR=0.89 (width/thickness) bar, showing comparison of measured and calculated impedance using discrete frequency and transient/FFT methods.

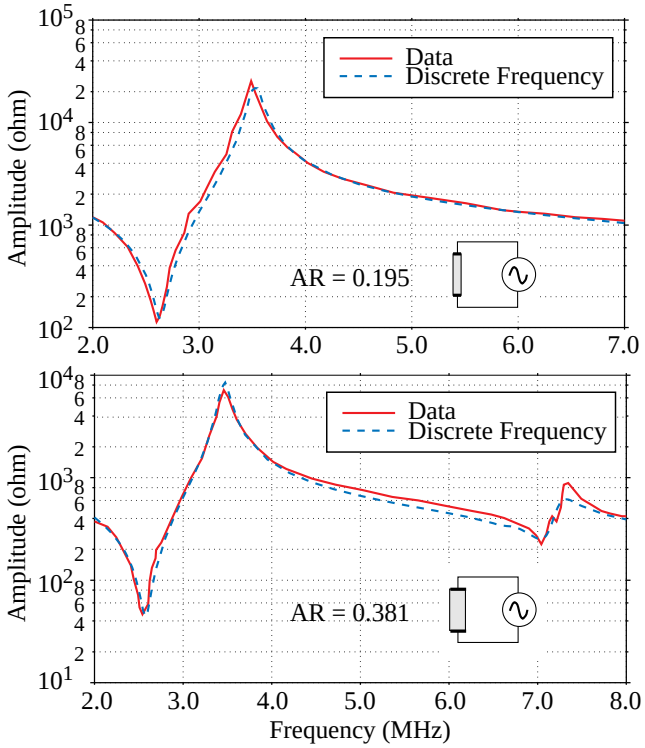

Figure 2. Electrical impedance amplitude for the AR=0.195 and 0.381 bars. Comparison of measured data and calculated impedance at discrete frequencies assuming a constant damping ratio of 1.89%.

variations showed that the stiffness coefficients were the most likely source of disagreement, e.g., increasing c_{13} by 4% aligned the lowest frequency extremals. Note that similarities in shape of impedance plots for the lowest and highest aspect ratios, ARs=0.195 (Fig. 2), 4.97 (Fig. 3) follow because both approach 1D behavior.

ARRAY SIMULATIONS

Useful models must accommodate the relatively complicated array structure of modern transducers. This includes stacks of piezoceramic, electrodes, adhesive, backing, matching layers, and lens material with filled or unfilled kerfs separating element stacks. The individual, albeit electromechanically coupled, transducer stacks are predominately 2D for kerfs in one direction or 3D for kerfs in two directions. Today, array design procedures typically rely on hybrid 1D models of individual elements [26, 27] and "mixture" models of composites [28]. However, there are important subtleties regarding acoustic coupling efficiency, cross-coupling between elements, radiation patterns, elemental mode shapes, etc., requiring both 2D and 3D numerical simulations.

To examine array applications we first considered a 2D finite element model of a hypothetical 1D transducer array. The stack consisted of backing material, a 0.3 mm PZT-5H layer, and a 0.125 mm matching layer. The array was defined by 0.05 mm wide, air-filled kerfs into the backing giving 0.1 mm wide piezoceramic bars on a 0.05 mm backing pedestal. Lens material (V_L=1.0 mm/μsec, ρ = 1.5 gm/cm^3) extended from the top of the stack. Two backing materials were considered, both with longitudinal impedance of 7.5 kg/sec/m^2 but one had twice the longitudinal wave speed (V_L=3.0 mm/μsec) and half the density (ρ = 2.5 gm/cm^3) of the other.

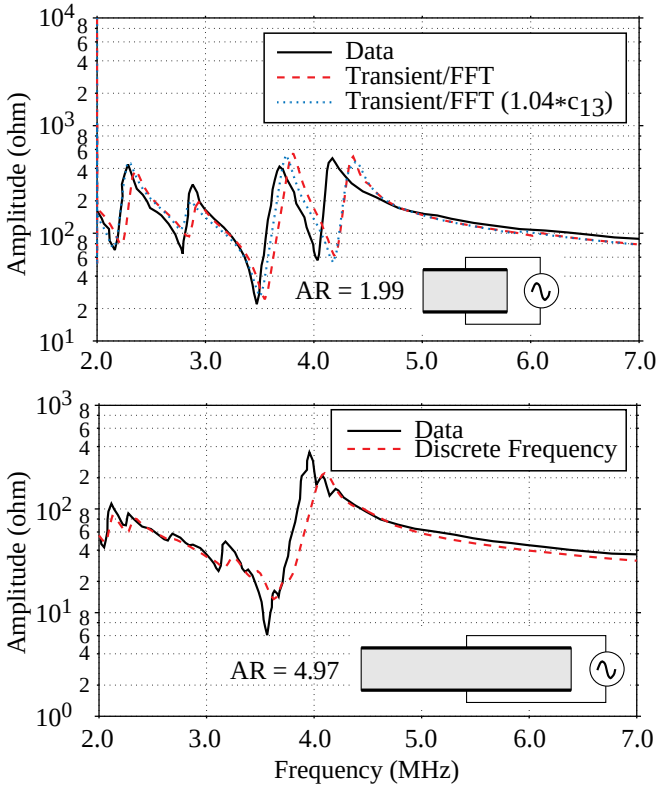

Figure 3. Electrical impedance amplitude for the AR=1.99 and 4.97 bars. Sensitivity to stiffness errors is indicated by perturbing the c_{13} coefficient +4% in the AR=1.99 model, which aligns the low frequency extrema.

The finite element model was made up of square 5.0x5.0 micrometer elements. The left boundary was a line of symmetry; the bottom, right, and top boundaries were absorbing (radiation conditions). The symmetry line bisected the center (driven) bar with 8 bars to its right—equivalent to a full model with 17 bars. The half-model was discretized into 260x370 = 96,200 2D square elements. Driving voltage was a 100 nsec smooth (C^1) pulse applied to electrodes (nodes) on the top and bottom faces of the center bar. Snapshots of the pressure over half of each model at 0.787 μsec are shown in Figure 4, with the faster backing case on the left. These are frames from an on-screen movie of transducer response that graphically illustrates the wave system and mechanical coupling across and between piezoelectric elements. Figure 5 displays plots of pressure time-histories and Fourier amplitude spectra for the fast and slow backing material, at a point in the lens 0.1 mm above the driven element on the centerline. The model required 76 cpu minutes (IBM RS/6000, Model 350) per μsec of simulation time.

A 3D example of the same stack model but with orthogonal kerfs defining 0.1x0.1x0.3 mm piezoceramic posts was also calculated. There were two planes of symmetry in this case and the model included two neighboring piezoceramic elements in each direction. The quarter-model consisted of 172x48x48 = 396,288 3D box elements measuring 7.0 to 8.3 micrometers on a side. The model and deformed shape (x60,000) of the stack and backing are drawn in Figure 6. This deformation pattern was for a sinusoidal driving voltage at 4.3 MHz. The 3D model took 7.2 cpu hours per μsec of simulation time (IBM RS/6000, Model 350).

WAVE PROPAGATION ISSUES

The previous examples emphasized transducer modeling. The *explicit* algorithm is well suited to wave propagation analysis in large-scale models with or without transduction elements. However, it should be emphasized that model size is constrained by available memory—severely so in 3D. Ten to fifteen elements per wave length are required to limit numerical wave dispersion caused by spatial discretization. Thus, in 2D (where the algorithm stores ≥5 words or ≥20 bytes per node) about 100x100

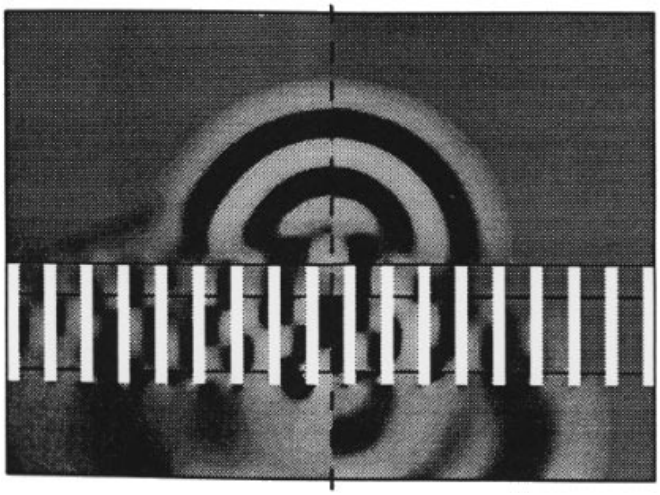

Figure 4. Snapshot of pressure over the symmetric 1D array at 0.787 μsec for two backing materials. Fast backing is on the left half and slow backing is on the right half. The center element is driven with a smooth 100 nsec pulse.

wave lengths can be modeled on a 64 Mbyte workstation. In sharp contrast, for 3D (where ≥7 words/node are stored) only about 10x10x10 wave lengths are feasible on the same machine.

There are two consequences of limited model size. First, very efficient radiation conditions are essential on the boundary of all all truncated materials (solids and fluids); otherwise the simulation does not correspond to the problem. Second, 3D wave studies must rely on wave field extrapolation for propagation across any significant span of homogeneous space surrounding the local 3D inhomogeneous model. Although large-scale 2D model studies are practical, extrapolation is still preferred across homogeneous space, for economy and to limit absolute phase errors. The mathematical basis for wave field extrapolation is Kirchhoff's integral representation for solutions of the inhomogeneous scalar wave equation, e.g., [29].

To illustrate wave propagation modeling we consider two applications in ultrasound therapy. The first concerns the interaction of ultrasound with bone in hyperthermia treatment. Figure 7 shows steady-state peak pressure calculated over a femur model insonified by a 500 kHz wave train (from above). There is strong coupling into the bone and focusing is apparent in the marrow. The second example concerns effects of wave nonlinearities at the beam focus in ultrasound tissue ablation. Figure 8 shows a 4 MHz beam from a cylindrical transducer (25 mm aperture, 30 mm focal length) focusing in a nonlinear fluid that exhibits "persistent" cavitation. Nonlinear density and stiffness changes are found to alter the post-focus pressure distribution significantly. Note, wave field extrapolation from the ultrasound source can be used to substantially reduce model size around these inhomogeneous or nonlinear regions.

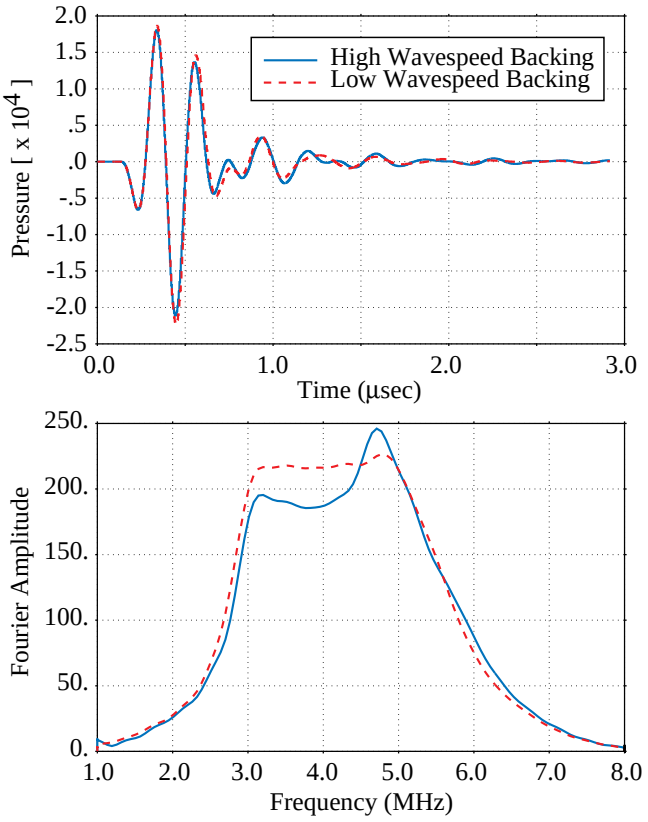

Figure 5. Plots of pressure time-histories and Fourier amplitude spectra for the fast backing and slow backing 1D array simulations. Output at a point 0.1 mm above the driven element.

SUMMARY AND CONCLUSIONS

In this paper we examined an *explicit* time-domain, finite element solution algorithm for the electromechanical equations describing piezoelectric transducers. We demonstrated an implementation of the algorithm for a variety of transducer and wave propagation problems and emphasized the substantial transient performance and 3D size advantages over more conventional *implicit* finite element algorithms (>100 for "complete" models). There are important aspects of the modeling

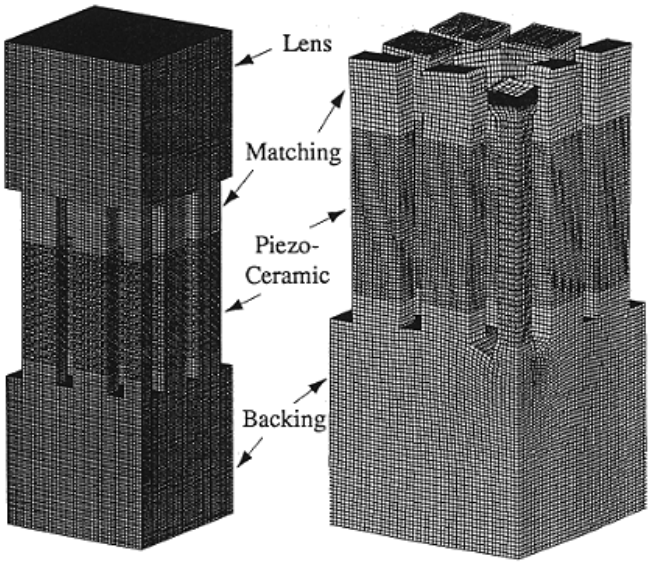

Figure 6. Finite element model of a 2D piezoelectric array with two planes of symmetry. The quarter model is shown on the left. An expanded view of the deformed shape (x60,000) for a 4.3 MHz driving voltage is shown on the right (lens removed).

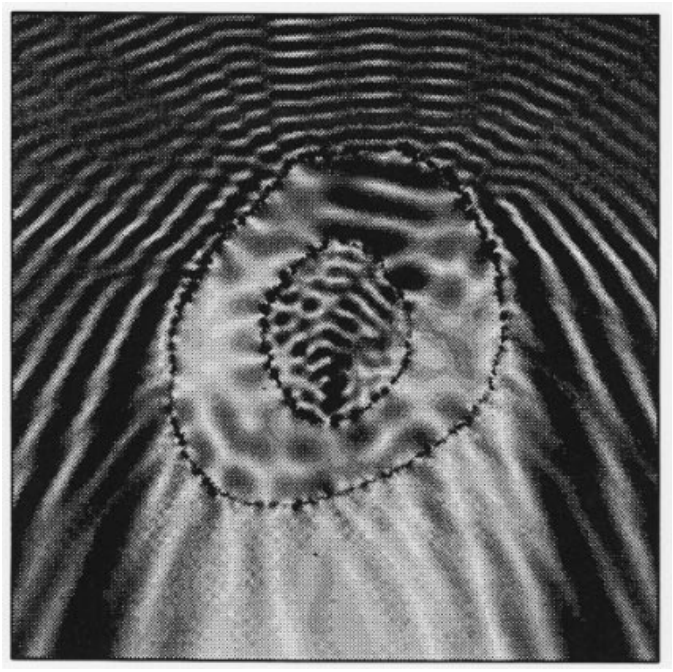

Figure 7. Steady-state pressure amplitude over a femur model insonified by a 500 kHz wave train from above. Dark is high pressure, light is low. Shows focusing in marrow and diffractions from step-wise approximation of bone interface.

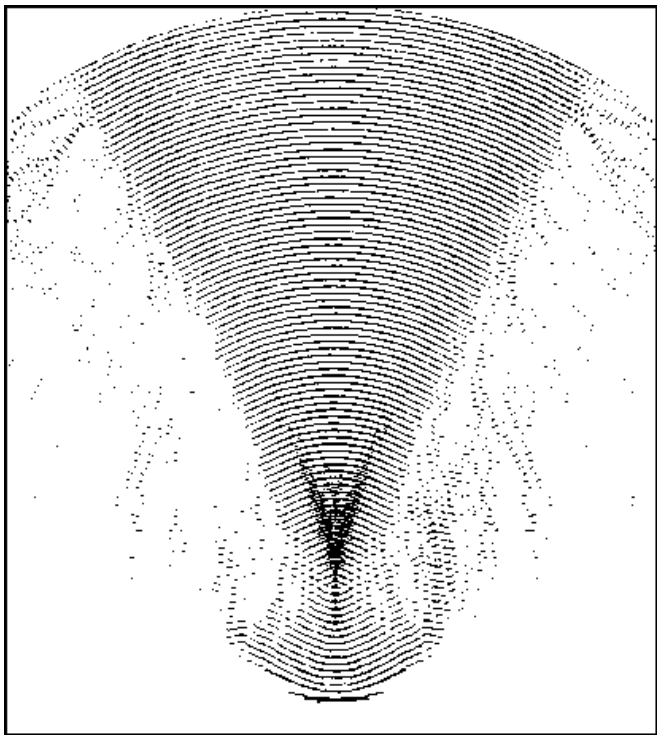

Figure 8. Beam from a 4 MHz cylindrical transducer (25 mm aperture, 30 mm focal length) focusing in a nonlinear fluid with "persistent" cavitation. Post-focus pressure is reduced by 40%.

problem that have not been touched on in this paper, e.g., transient driver circuit modeling, structural models (shells, beams, membranes) for subgrid features like adhesive, electrodes, etc., shock modeling in water, and last but not least, the reception problem. All of these will be addressed in the course of our NSF-sponsored research. Finite element eigen-analysis, e.g., [30], also deserves attention, specifically, the feasibility of extracting eigen-data from time-domain solutions.

Explicit time-domain wave solvers are by no means new, e.g., [31]. They have been widely used for shock problems in continua (finite difference) and structures (finite element) for well over 30 years, but almost exclusively in weapons-related applications. Nonetheless, their application to piezoelectric transducers has required significant modification of the conventional *explicit* approach. Issues include the appropriate mixing of *explicit* mechanical and *implicit* electrical solvers and proper coupling of the *explicit* velocity potential (acoustic) and displacement (elastic) elements. It should be noted that the mixed algorithm described here can be extended to coupled mechanical wave propagation, heat generation, and heat diffusion (bioheat) problems. This capability would be useful in transducer design, hyperthermia and tissue ablation models, and FDA regulatory reporting [32].

In conclusion, the *explicit* transducer modeling algorithm described here was demonstrated to be both effective and practical for wave propagation analysis in electromechanical structures and continua. It has always been available to analysts but was overshadowed by *implicit* approaches for historical and technical reasons. This should no longer be the case given the speed and model size advantages of *explicit* integration. With current workstations (and future PCs), this algorithm permits desktop design simulations that required a supercomputer four years ago. Nonetheless, do better algorithms exist? In principle the answer is yes. The Fourier (pseudospectral) method or high order finite elements achieve good propagation accuracy with ≤ 5 nodes per wave length versus ≈ 15 for the low order element. However, in practice these schemes exhibit poor model resolution since fewer nodes are available to define interfaces. Future research might consider a combination of low order and high order elements where needed. All simulation results in this paper were calculated using the PZFlex finite element code [33].

ACKNOWLEDGEMENTS

The authors wish to thank Dr. John Fraser at ATL for the impedance measurements, Prof. Charles Cain at University of Michigan for the tissue model, and Dr. Claudio Zanelli at Intec for information on focused ultrasound. This research was supported in part under NSF SBIR grant ISI 9161050.

REFERENCES

[1] G.S. Kino, Acoustic Waves, Prentice-Hall Inc., 1987.

[2] P. Fish, Physics and Instrumentation of Diagnostic Medical Ultrasound, John Wiley & Sons, 1990.

[3] H. Allik and T.J.R. Hughes, "Finite element method for piezoelectric vibration," *Int. Numer. Methods Engng.*, **2**, 151-157, 1970.

[4] H. Allik, K.M. Webman, and J.T. Hunt, "Vibrational response of sonar transducers using piezoelectric finite elements," *J. Acoust. Soc. Am.*, **56,** 1782-1792, 1974.

[5] Y. Kagawa and T. Yamabuchi, "Finite element simulation of two-dimensional electromechanical resonators," *IEEE Trans. Sonics Ultrason.*, **SU-21**, 1974.

[6] Y. Kagawa and T. Yamabuchi, "Finite element simulation of a composite piezoelectric ultrasonic transducer," *IEEE Trans. Sonics Ultrason.*, **SU-26**, 81-88, 1979.

[7] D. Boucher, M. Langier, and C. Maerfeld, "Computation of the vibrational modes for piezoelectric array transducers using a mixed finite element-perturbation method," *IEEE Trans. Sonics Ultrason.*, **SU-28**, 318-330, 1981.

[8] M. Naillon, R. Coursant, and F. Besnier, "Analysis of piezoelectric structures by a finite element method," *Acta Electronica*, **25**, 341-362, 1983.

[9] G.F. McDearmon, "The addition of piezoelectric properties to structural finite element programs by matrix manipulations," *J. Acoust. Soc. Am.*, **76**, 1984.

[10] P.C. Kohnke, ANSYS® Engineering Analysis System Theoretical Manual, Swanson Analysis Systems, Inc., P.O. Box 65, Houston, Pennsylvania 15342.

[11] R. Lerch, "Finite element analysis of piezoelectric transducers," *Proc. IEEE Ultrasonic Symp.*, **2**, 643-654, 1988.

[12] R. Lerch, "Simulation of piezoelectric devices by two- and three-dimensional finite elements," *IEEE Trans. Sonics Ultrason.*, **SU-37**, 233-247, 1990.

[13] D. Ranlet, F. DiMaggio, H. Bleich, M. Baron, "Elastic response of submerged shells with internally attached structures to shock loading," *Comput. Struct.*, **7**, 1977.

[14] G.L. Wojcik, D.K. Vaughan, M. Barenberg, J. Mould, and M.B. Hulit, "Large-scale, explicit wave simulations on the CRAY-2," *Applied Num. Math.*, **4**, 47-70, 1988.

[15] Computational Methods for Transient Analysis, Vol. 1 in *Computational Methods in Mechanics*, T. Belytschko and T.J.R. Hughes (Eds.), Elsevier Science Publishers B.V. 1983.

[16] G.L. Wojcik, D.K. Vaughan, and N. Abboud, "Electromechanical finite element models for ultrasound transducer analysis and design," NSF SBIR Phase I Report, ISI 9161050, 1993.

[17] B.A. Auld, Acoustic Fields and Waves in Solids, Vol. 1, 2nd edition, Krieger, 1990.

[18] R.D. Richtmeyer and K.W. Morton, Difference Methods for Initial-Value Problems, Interscience Publishers, 1957.

[19] R.H. Burkhart and D.P. Young, "GMRES acceleration and optimization codes," ETA-TR-88, Boeing Computer Services, May 1988.

[20] R.W. Freund, "Conjugate gradient type methods for linear systems with complex symmetric coefficient matrices," *SIAM J. Sci. Stat. Computing*, **13**, No.1, 1992.

[21] R. Courant, K.O. Friedrichs, and H. Lewy, "Über die partiellen differenzengleichungen der mathematischen physik," *Math. Ann.*, **100**, 32, 1928.

[22] H. Kolsky, Stress Waves in Solids, Dover Publications, Inc., 1963.

[23] D. Givoli, "Non-reflecting boundary conditions: a review," *J. Comput. Phys.*, 94-129, 1991.

[24] I. Sandler, "A new procedure for analyzing structure-medium interaction," DNA Numerical Methods Symposium, Menlo Park, California, April 1992.

[25] R. Clayton and B. Enquist, "Absorbing boundary conditions for acoustic and elastic wave equations," *Bull. Seism. Soc. Am.*, **67**, 1529-1540, 1977.

[26] R. Krimholtz, D.A. Leedom, and G.L. Matthaei, "New equivalent circuits for elementary piezoelectric transducers," *Electron. Lett.*, **6**, No.13, 398-399, 1970.

[27] M. Redwood, "Transient performance of a piezoelectric transducer," *J. Acost. Soc. Am.*, **33**, No.4, 527-536, 1961.

[28] W.A. Smith and B.A. Auld, "Modeling 1-3 composite piezoelectrics: thickness-mode oscillations," *IEEE Trans. Ultrason. Ferroelec. Freq. Contr.*, **38**, 40-47, 1991.

[29] J.A. Stratton, Electromagnetic Theory, McGraw-Hill Book Co., 1941.

[30] H.A. Kunkel, S. Locke, and B. Pikeroen, "Finite-element analysis of vibrational modes in piezoelectric ceramic disks," *IEEE Trans. Ultrason. Ferroelec. Freq. Contr.*, **37**, 316-328, 1990.

[31] J. von Neumann and R.D. Richtmyer, "A method for the numerical calculation of hydrodynamical shocks," *J. Appl Phys.*, **21**, 232, 1950.

[32] K.E. Thomenius, "Thermal dosimetry models for diagnostic ultrasound," *Proc. IEEE Ultrason. Symp.*, 1399-1408, 1990.

[33] D.K. Vaughan and E. Richardson, FLEX User's Guide, Weidlinger Associates, 1993.